

Alternatives for the scalar sector of the Standard Model after the LHC discovery

Bohdan GRZADKOWSKI
University of Warsaw

- The LHC data
- Gravity-Higgs mixing (the off-brane RS setup)
 - The model
 - Results
- Second Higgs doublet
 - Type I and II models
 - Strategy: scanning and experimental constraints
 - Results
- Summary
 - ◊ B.G., J. F. Gunion and M. Toharia, "Higgs-Radion interpretation of the LHC data?" Phys. Lett. B **712**, 70 (2012),
 - ◊ D. Dominici, B.G., J. F. Gunion and M. Toharia, "The Scalar sector of the Randall-Sundrum model", Nucl. Phys. B **671**, 243 (2003),
 - ◊ A. Drozd, B.G., J. Gunion and Y. Jiang, "Two-Higgs Doublet Models and Enhanced Rates for a 125 GeV Higgs", in progress.

The LHC data

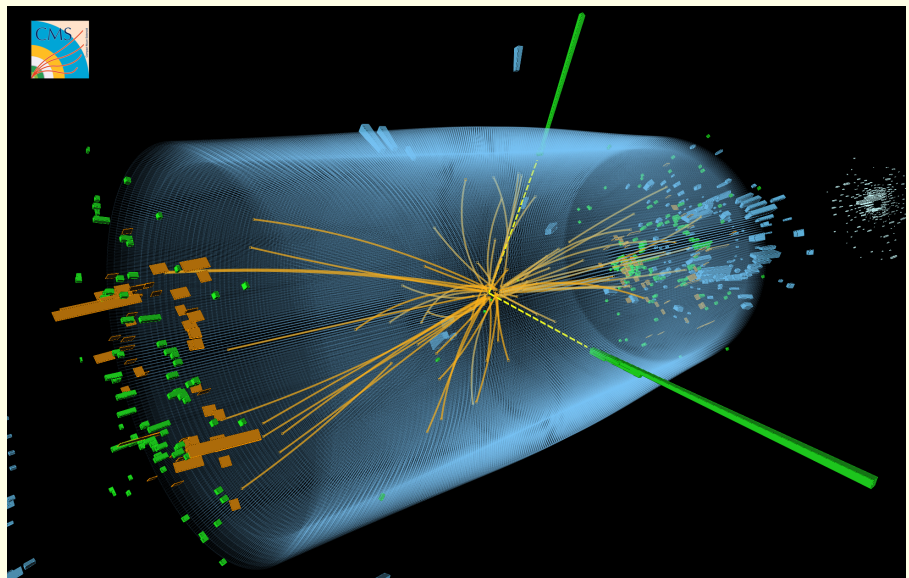
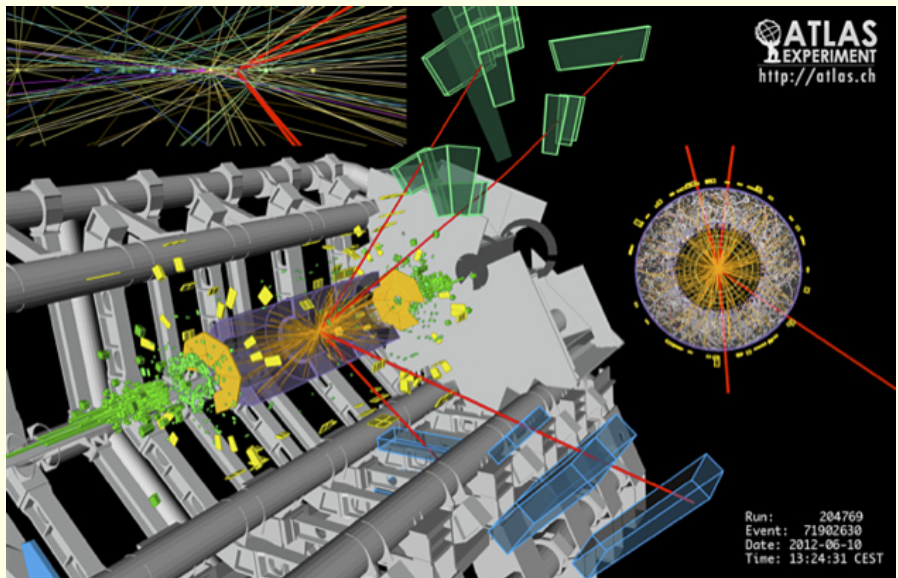


Figure 1: 1) Candidate Higgs Decay to four muons ($h \rightarrow ZZ \rightarrow 4\mu$) recorded by ATLAS in 2012. 2) Event recorded by CMS in 2012. The event shows characteristics expected from a decay of the SM Higgs boson to a pair of photons (dashed yellow lines and green towers): $h \rightarrow \gamma\gamma$.

- G. Aad *et al.* [ATLAS Collaboration], “Observation of a new particle in the search for the Standard Model Higgs boson with the ATLAS detector at the LHC”, [arXiv:1207.7214 [hep-ex]].
- S. Chatrchyan *et al.* [CMS Collaboration], “Observation of a new boson at a mass of 125 GeV with the CMS experiment at the LHC”, [arXiv:1207.7235 [hep-ex]].

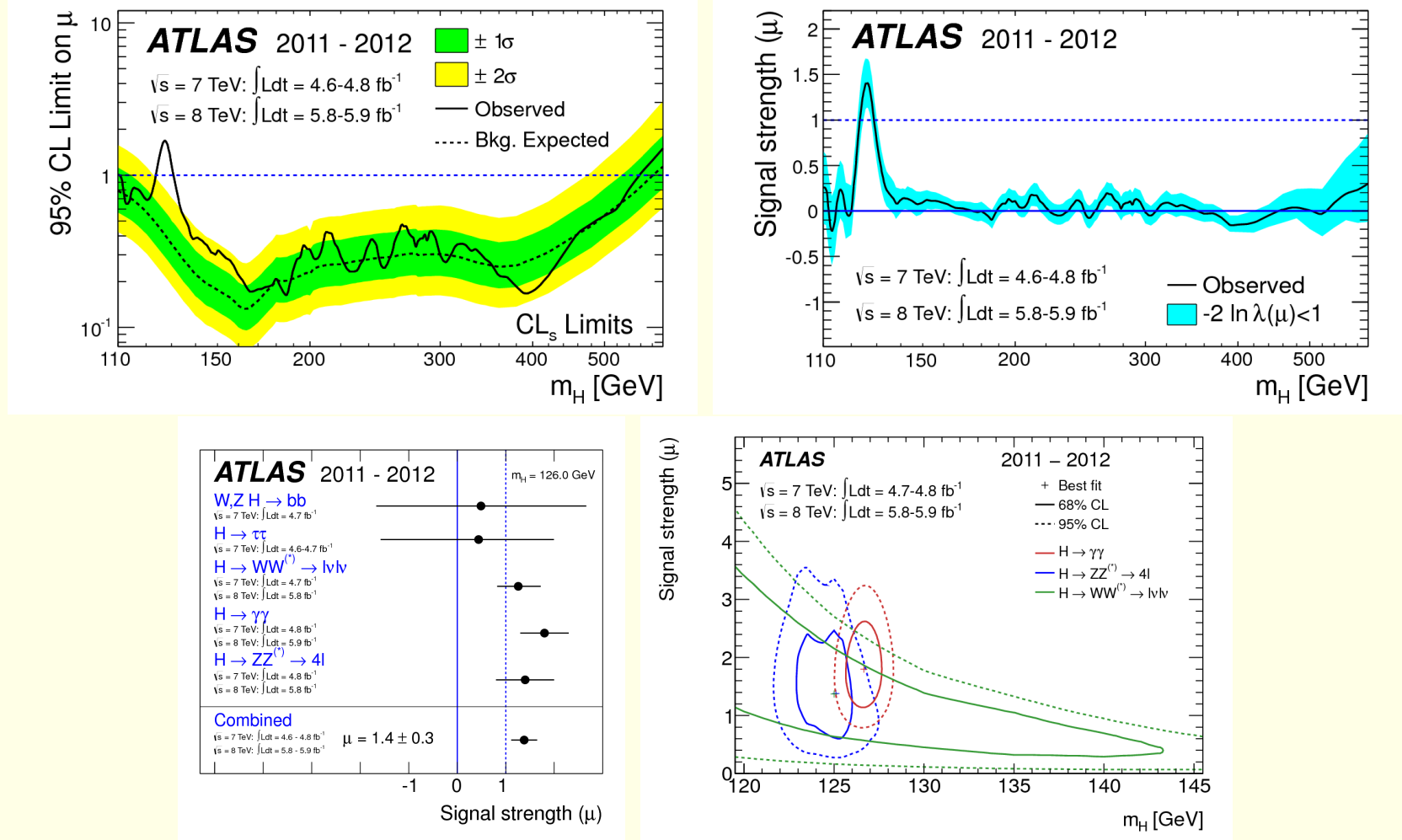


Figure 2: 1) The observed (solid) 95% CL upper limit on the signal strength as a function of m_h and the expectation (dashed) under the background-only hypothesis. The green and yellow bands show the $\pm 1\sigma$ and $\pm 2\sigma$ uncertainties on the background-only. 2) The best-fit signal strength μ as a function of m_h . The band indicates the approximate 68% CL interval around the fitted value. 3) Measurements of the signal strength parameter μ for $m_h = 126 \text{ GeV}$ for the individual channels and their combination. 4) Confidence intervals in the (μ, m_h) plane for the $h \rightarrow ZZ^{(*)} \rightarrow 4l$, $h \rightarrow \gamma\gamma$, and $h \rightarrow WW^{(*)} \rightarrow l\nu l\nu$ channels, including all systematic uncertainties. The markers indicate the maximum likelihood estimates in the corresponding channels.

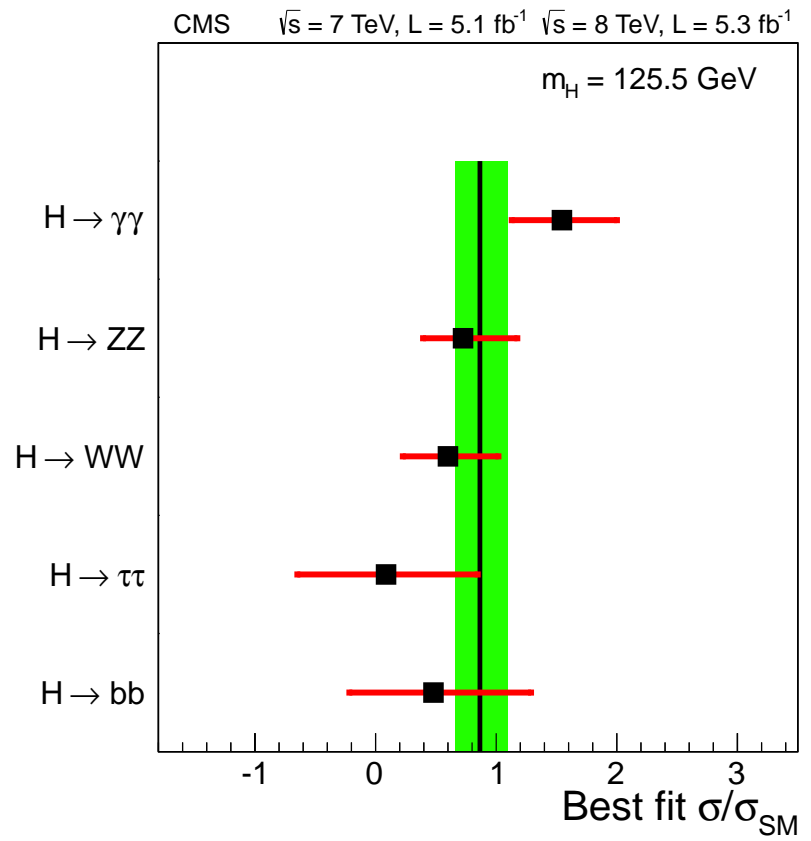
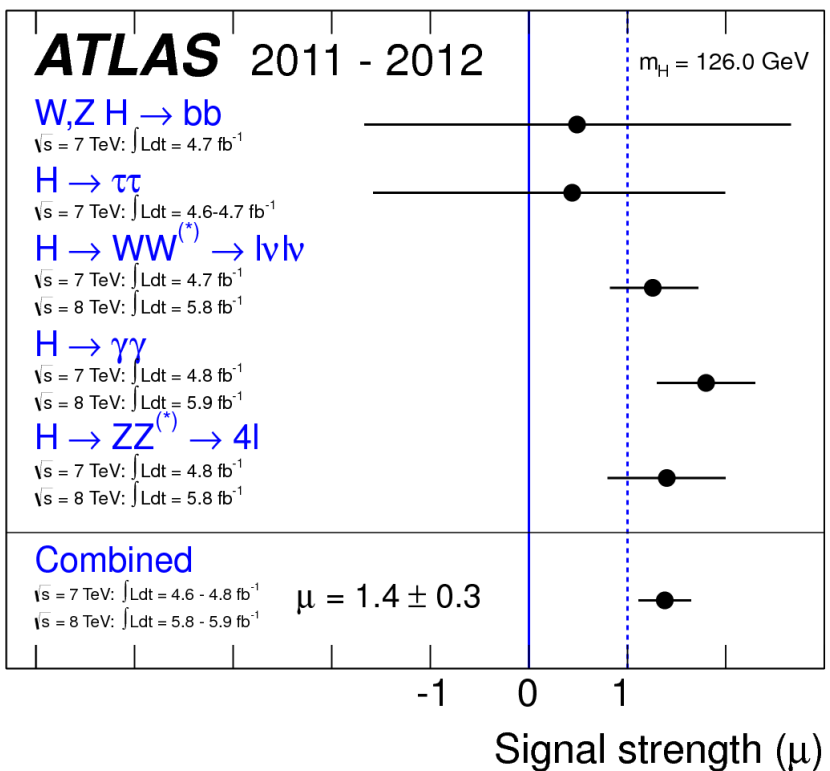


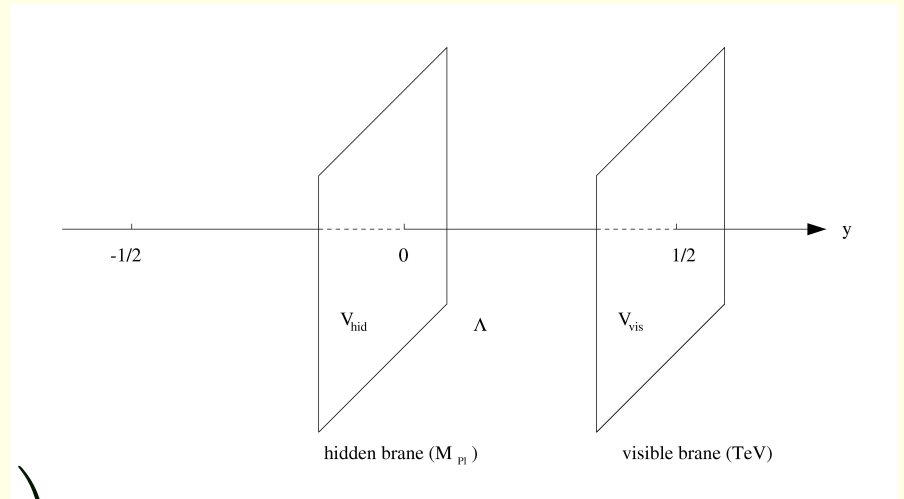
Figure 3: Comparison of ATLAS and CMS results. The vertical green band for CMS shows the overall σ/σ_{SM} value 0.87 ± 0.23 .

Gravity-Higgs mixing (the off-brane RS setup)

- 3 space, 1 time (x^μ), + 1 extra spatial dimension (y), orbifold: $y \equiv y + 1$, $y \equiv -y$
- Standard Model particles on a “visible” brane (at $y = 1/2$),
- Planck mass scale physics on the “hidden” (at $y = 0$),
- Gravity in the bulk (for any y),

The full 5d action ($\epsilon^2 \equiv m_{Pl5}^{-3}$):

$$\begin{aligned}
 S &= - \int d^4x dy \sqrt{-\hat{g}} \left(\frac{\hat{R}}{\epsilon^2} + \Lambda \right) \\
 &\quad + \int d^4x \sqrt{-g_{\text{hid}}} (\mathcal{L}_{\text{hid}} - V_{\text{hid}}) + \int d^4x \sqrt{-g_{\text{vis}}} (\mathcal{L}_{\text{vis}} - V_{\text{vis}})
 \end{aligned}$$



Strategy:

- Solution of the Einstein's equations:

$$ds^2 = e^{-2m_0 b_0 |y|} \eta_{\mu\nu} dx^\mu dx^\nu - b_0^2 dy^2$$

for

$$V_{\text{hid}} = -V_{\text{vis}} = \frac{12m_0}{\epsilon^2} \quad \text{and} \quad \Lambda = -\frac{12m_0^2}{\epsilon^2}$$

- An expansion around the background metric:

- $\eta_{\mu\nu} \rightarrow \eta_{\mu\nu} + \epsilon h_{\mu\nu}(x, y)$,
- $b_0 \rightarrow b_0 + b(x)$,

$$h_{\mu\nu}(x, y) = \sum_n h_{\mu\nu}^n(x) \frac{\chi^n(y)}{\sqrt{b_0}} \quad \Rightarrow \quad \mathcal{L}_{\text{int}} = -\frac{1}{\Lambda_W} \sum_{n \neq 0} h_{\mu\nu}^n T^{\mu\nu} - \frac{\phi_0}{\Lambda_\phi} T_\mu^\mu$$

for

$$\Lambda_W \simeq \sqrt{2} m_{Pl} \Omega_0, \quad \Lambda_\phi = \sqrt{3} \Lambda_W, \quad \Omega_0 = e^{-m_0 b_0 / 2} \quad \text{and} \quad \phi_0(x) \equiv \sqrt{6} m_{Pl} e^{-m_0 (b_0 + b(x)) / 2}$$

$$S_\xi = \xi \int d^4x \sqrt{g_{\text{vis}}} R(g_{\text{vis}}) H^\dagger H,$$

where $R(g_{\text{vis}})$ is the Ricci scalar for the metric induced on the visible brane.

$$\mathcal{L}_{\text{kin}} = -\frac{1}{2}(1 + 6\gamma^2\xi)\phi_0 \square \phi_0 - \frac{1}{2}\phi_0 m_{\phi_0}^2 \phi_0 - \frac{1}{2}h_0(\square + m_{h_0}^2)h_0 - 6\gamma\xi\phi_0 \square h_0,$$

where $\gamma \equiv v_0/\Lambda_\phi$

$$\tan 2\theta \equiv 12\gamma\xi Z \frac{m_{h_0}^2}{m_{\phi_0}^2 - m_{h_0}^2(Z^2 - 36\xi^2\gamma^2)} \quad \text{for } Z^2 \equiv 1 + 6\xi\gamma^2(1 - 6\xi)$$

Canonically normalized states that diagonalize the kinetic energy are h and ϕ :

$$\begin{aligned} h_0 &= \left(\cos \theta - \frac{6\xi\gamma}{Z} \sin \theta \right) h + \left(\sin \theta + \frac{6\xi\gamma}{Z} \cos \theta \right) \phi \\ \phi_0 &= -\cos \theta \frac{\phi}{Z} + \sin \theta \frac{h}{Z} \end{aligned}$$

Remarks:

- The RS model provides a simple solution to the hierarchy problem if the Higgs is placed on the TeV brane at $y = 1/2$ by virtue of the fact that the 4D electro-weak scale v_0 is given in terms of the $\mathcal{O}(m_{Pl})$ 5D Higgs vev, \hat{v} , by:

$$v_0 = \Omega_0 \hat{v} = e^{-\frac{1}{2}m_0 b_0} \hat{v} \sim 1 \text{ TeV} \quad \text{for} \quad \frac{1}{2}m_0 b_0 \sim 35$$

As a result, to solve the hierarchy problem, $\Lambda_\phi = \sqrt{6}m_{Pl}\Omega_0$ should be of order $1 - 10$ TeV, but not much higher

- non-unitarity

$$g_{ZZh}^2 + g_{ZZ\phi}^2 = 1 + \frac{\gamma^2(1 - 6\xi)^2}{Z^2}$$

Higher-dimensional operators in the 5D effective field theory are suppressed only by TeV^{-1} and then FCNC processes and PEW observable corrections are predicted to be much too large.



It is therefore now regarded as necessary to allow all the SM fields (except the Higgs) to propagate in the extra dimension. The SM particles are then the zero-modes of the 5D fields and the profile of a SM fermion in the extra dimension can be adjusted using a mass parameter.

For example, for the W we have (before mixing)

$$\mathcal{L} \ni h_0 \frac{2m_W^2}{v} W_\mu^\dagger W^\mu - \phi_0 \frac{2m_W^2}{\Lambda_\phi} \left[W_\mu^\dagger W^\mu (1 - \kappa_W) + W_{\mu\nu}^\dagger W^{\mu\nu} \frac{1}{4m_W^2 (\frac{1}{2} m_0 b_0)} \right]$$

where $\kappa_V = \left(\frac{3m_V^2 (\frac{1}{2} m_0 b_0)}{\Lambda_\phi^2 (m_0/m_{Pl})^2} \right)$ for $V = W, Z$.

After mixing, this becomes, for example for the h interaction

$$\mathcal{L} \ni h \frac{2m_W^2}{v} \left[g_h^W W_\mu^\dagger W^\mu + g_h^r \frac{1}{4m_W^2 (\frac{1}{2} m_0 b_0)} W_{\mu\nu}^\dagger W^{\mu\nu} \right]$$

with a similar result for the ϕ .

$$m_1^g = \frac{x_1^g}{\sqrt{6} m_{Pl}} \Lambda_\phi \quad \text{for} \quad x_1^g = 2.45$$

Scenarios:

- A strong lower bound on the masses of the first excitations of the gauge bosons applies (CMS): $m_1^g \geq 1.5 \text{ TeV}$ (K. Agashe *et al.*, Phys. Rev. D **77**, 015003 (2008))
When $m_1^g \geq 1.5 \text{ TeV}$ then

$$\Lambda_\phi \lesssim 10 \text{ TeV} \Rightarrow \frac{m_0}{m_{Pl}} \gtrsim 0.15$$

Thus, a significant lower bound on m_1^g implies that only relatively large values for m_0/m_{Pl} are allowed. For phenomenology we adopt (fixed m_1^g):

$$\Lambda_\phi = m_1^g \frac{\sqrt{6}}{x_1^g} \left(\frac{m_0}{m_{Pl}} \right)^{-1}$$

- Fermionic profiles (flat for light quarks) are such that bounds on gauge boson excitations are very weak. Then no substantial experimental limits on m_1^g could be obtained (fixed Λ_ϕ adopted).

Table 1: The LHC excesses in the $\gamma\gamma$ and 4ℓ final states.

	$R(\gamma\gamma)$	$R(4\ell)$
ATLAS	$\sim 1.8^{+0.4}_{-0.4}$	$\sim 1.4^{+0.6}_{-0.6}$
CMS	$\sim 1.5^{+0.5}_{-0.5}$	$\sim 0.7^{+0.5}_{-0.4}$

$$R_h(X) \equiv \frac{\Gamma_h(gg)BR(h \rightarrow X)}{\Gamma_{h_{SM}}(gg)BR(h_{SM} \rightarrow X)}, \quad R_\phi(X) \equiv \frac{\Gamma_\phi(gg)BR(\phi \rightarrow X)}{\Gamma_{h_{SM}}(gg)BR(h_{SM} \rightarrow X)},$$

$$X = \gamma\gamma, ZZ, b\bar{b}$$

Signals

- Signal at only 125 GeV
- Signal (h or ϕ) at 125 GeV and high mass $m_\phi \gtrsim 500$ GeV

Signal at only 125 GeV ($m_1^g = 1.5$ TeV)

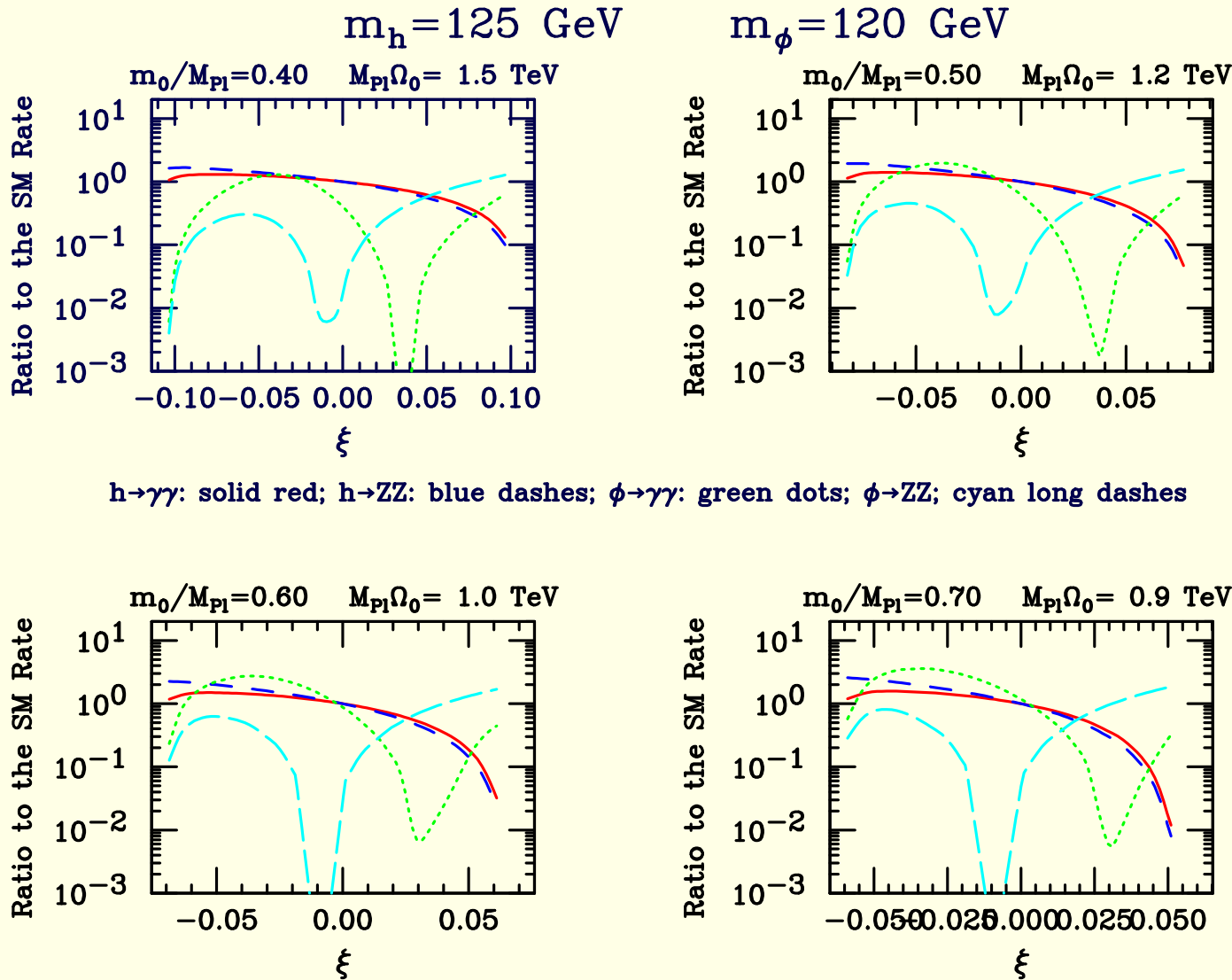


Figure 4: For $m_h = 125$ GeV and $m_\phi = 120$ GeV, we plot $R_h(X)$ and $R_\phi(X)$ for $X = \gamma\gamma$ and $X = ZZ$ (equivalent to $X = 4\ell$) as a function of ξ , assuming $m_1^g = 1.5$ TeV.

Signal (h or ϕ) at 125 GeV and high mass ($m_1^g = 1.5$ TeV)

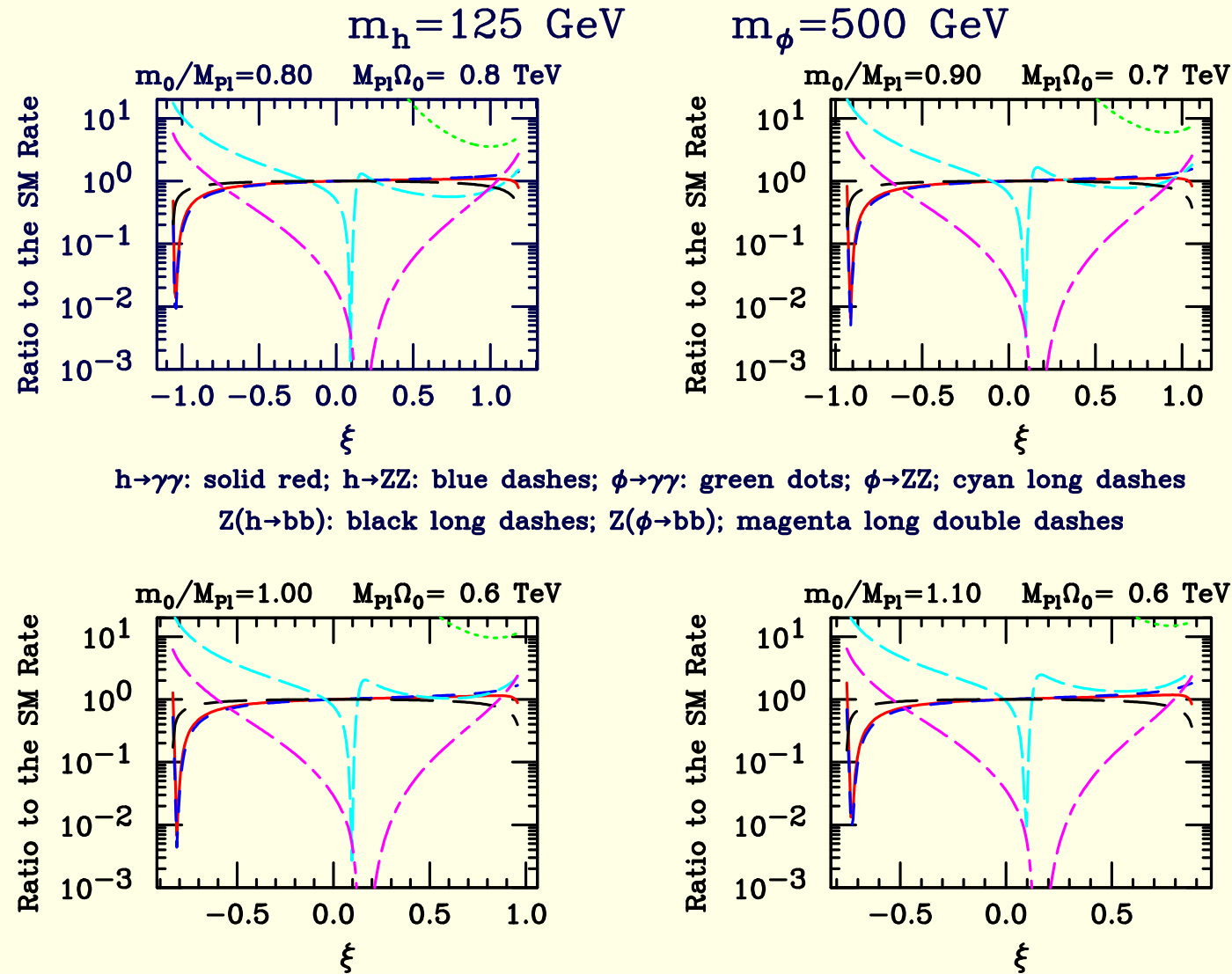


Figure 5: For $m_h = 125$ GeV and $m_\phi = 500$ GeV, we plot $R_h(X)$ and $R_\phi(X)$ for $X = \gamma\gamma$ and $X = ZZ$ (equivalent to $X = 4l$) as a function of ξ , assuming $m_1^g = 1.5$ TeV. Also shown are the similarly defined ratios for $Z + h$ production with $h \rightarrow b\bar{b}$ and $Z + \phi$ production with $\phi \rightarrow b\bar{b}$.

Signal at only 125 GeV (fixed $\Lambda_\phi = 1$ TeV)

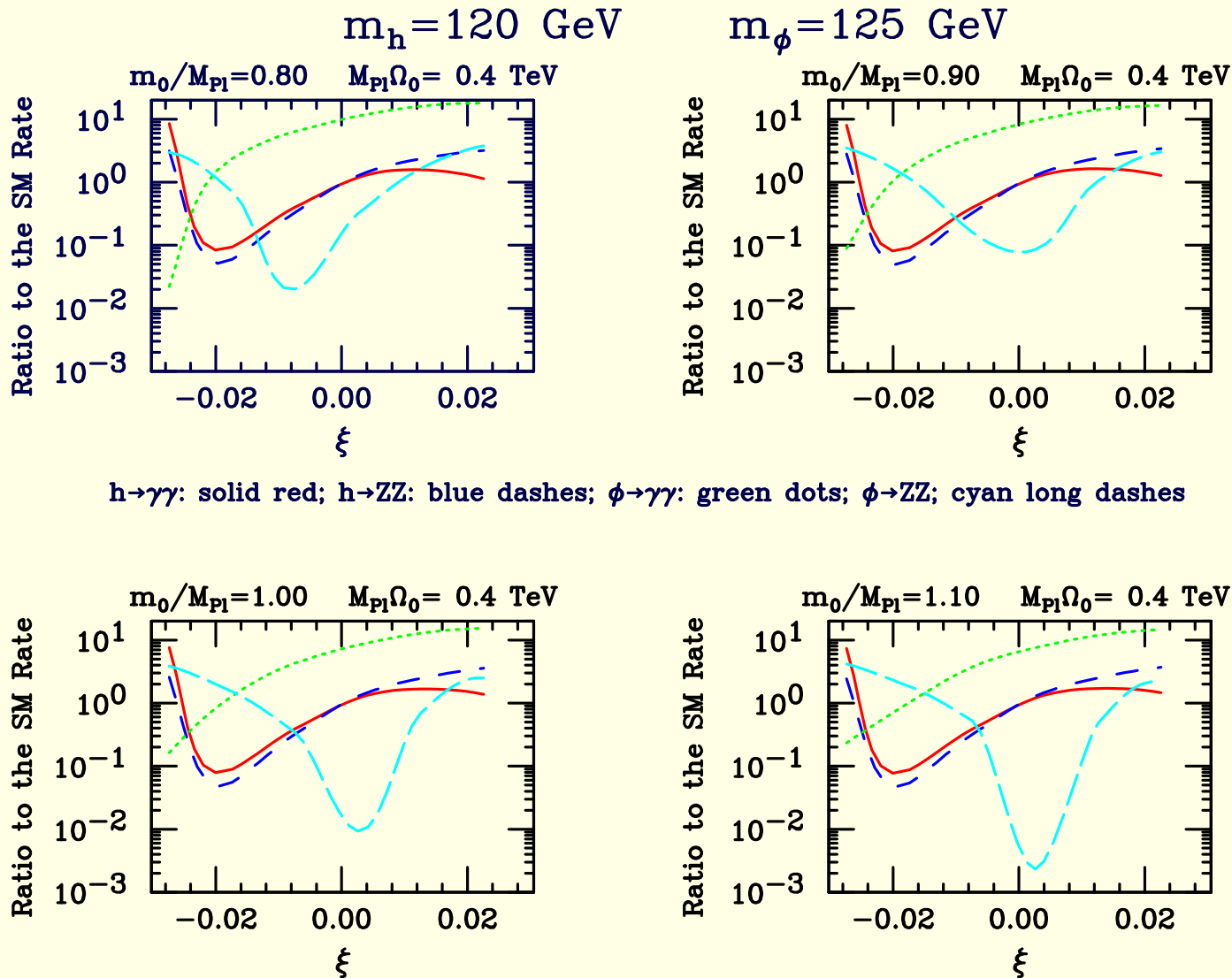


Figure 6: For $m_h = 120$ GeV and $m_\phi = 125$ GeV, we plot $R_h(X)$ and $R_\phi(X)$ for $X = \gamma\gamma$ and $X = ZZ$ (equivalent to $X = 4\ell$) as a function of ξ taking Λ_ϕ fixed at 1 TeV.

Conclusions on the Gravity-Higgs mixing setup:

- Fixed $m_1^g = 1.5$ TeV scenario:
 - Signal at only 125 GeV: consistent parameters could be found for $m_h = 125$ GeV and $m_\phi = 120$ GeV: e.g. $m_0/m_{Pl} = 0.4$ and $\xi \sim -0.09$.
 - Signal (h or ϕ) at 125 GeV and high mass: too large $|\xi|$ is needed (difficulties with precision electroweak constraints).
- Fixed $\Lambda_\phi = 1$ TeV scenario:
 - Signal at only 125 GeV: consistent parameters could be found for $m_h = 120$ GeV and $m_\phi = 125$ GeV: e.g. $m_0/m_{Pl} = 1$ and $\xi \sim -0.016$.
 - Signal (h or ϕ) at 125 GeV and high mass: no consistent and interesting solution.

Second Higgs doublet

♠ Type I and II models

$$\begin{aligned}
 V(\Phi_1, \Phi_2) = & m_{11}^2 \Phi_1^\dagger \Phi_1 + m_{22}^2 \Phi_2^\dagger \Phi_2 - \left[m_{12}^2 \Phi_1^\dagger \Phi_2 + \text{h.c.} \right] \\
 & + \frac{\lambda_1}{2} \left(\Phi_1^\dagger \Phi_1 \right)^2 + \frac{\lambda_2}{2} \left(\Phi_2^\dagger \Phi_2 \right)^2 + \lambda_3 \left(\Phi_1^\dagger \Phi_1 \right) \left(\Phi_2^\dagger \Phi_2 \right) + \lambda_4 \left(\Phi_1^\dagger \Phi_2 \right) \left(\Phi_2^\dagger \Phi_1 \right) \\
 & + \left\{ \frac{\lambda_5}{2} \left(\Phi_1^\dagger \Phi_2 \right)^2 + \left[\lambda_6 \left(\Phi_1^\dagger \Phi_1 \right) + \lambda_7 \left(\Phi_2^\dagger \Phi_2 \right) \right] \left(\Phi_1^\dagger \Phi_2 \right) + \text{h.c.} \right\}.
 \end{aligned}$$

$$\langle \Phi_1 \rangle = \frac{v}{\sqrt{2}} \begin{pmatrix} 0 \\ \cos \beta \end{pmatrix} \quad \langle \Phi_2 \rangle = \frac{v}{\sqrt{2}} \begin{pmatrix} 0 \\ e^{i\xi} \sin \beta \end{pmatrix},$$

where $v = (\sqrt{2}G_F)^{-1/2} \approx 246$ GeV and $\xi = 0$.

$$\Phi_a = \begin{pmatrix} \phi_a \\ (v_a + \rho_a + i\eta_a)/\sqrt{2} \end{pmatrix} \quad a = 1, 2$$

with $v_1 = v \cos \beta$ and $v_2 = v \sin \beta$.

The neutral Goldstone boson

$$G^0 = \eta_1 \cos \beta + \eta_2 \sin \beta$$

The physical pseudoscalar

$$A = -\eta_1 \sin \beta + \eta_2 \cos \beta$$

The physical scalars are:

$$h = -\rho_1 \sin \alpha + \rho_2 \cos \alpha, \quad H = \rho_1 \cos \alpha + \rho_2 \sin \alpha$$

The LHC signal normalized to the SM prediction

$$R_{gg}^{h_i}(X) \equiv \frac{\Gamma(gg \rightarrow h_i) \ BR(h_i \rightarrow X)}{\Gamma(gg \rightarrow h_{SM}) \ BR(h_{SM} \rightarrow X)}$$

for $X = \gamma\gamma, ZZ, b\bar{b}$ and $h_i = h, H, \dots$

Earlier works:

- P. M. Ferreira, R. Santos, M. Sher and J. P. Silva, “Could the LHC two-photon signal correspond to the heavier scalar in two-Higgs-doublet models?,” Phys. Rev. D **85**, 035020 (2012) [arXiv:1201.0019 [hep-ph]].
- P. M. Ferreira, R. Santos, M. Sher and J. P. Silva, “Implications of the LHC two-photon signal for two-Higgs-doublet models,” Phys. Rev. D **85**, 077703 (2012) [arXiv:1112.3277 [hep-ph]].

$$\mathcal{L}_Y^{(q)} = \bar{Q}_L \tilde{\Gamma}_1 u_R \tilde{\Phi}_1 + \bar{Q}_L \Gamma_1 d_R \Phi_1 + \bar{Q}_L \tilde{\Gamma}_2 u_R \tilde{\Phi}_2 + \bar{Q}_L \Gamma_2 d_R \Phi_2 + \text{H.c.}$$

then

$$M_u = -\tilde{\Gamma}_1 \langle \tilde{\Phi}_1 \rangle - \tilde{\Gamma}_2 \langle \tilde{\Phi}_2 \rangle \quad M_d = -\Gamma_1 \langle \Phi_1 \rangle - \Gamma_2 \langle \Phi_2 \rangle$$

Natural Flavour Conservation:

- Type I model, \mathbb{Z}_2 softly broken (by $m_{12}^2 \neq 0$): $\Phi_1 \rightarrow -\Phi_1 \Rightarrow \lambda_6 = \lambda_7 = 0$
- Type II model, \mathbb{Z}_2 softly broken (by $m_{12}^2 \neq 0$): $\Phi_1 \rightarrow -\Phi_1$ and $d_R \rightarrow -d_R \Rightarrow \lambda_6 = \lambda_7 = 0$

Table 2: Fermionic coupling patterns for Type I and Type II two-Higgs-doublet models.

Higgs	Type I			Type II		
	up quarks	down quarks	leptons	up quarks	down quarks	leptons
h	$\cos \alpha / \sin \beta$	$-\sin \alpha / \cos \beta$	$-\sin \alpha / \cos \beta$			
H	$\sin \alpha / \sin \beta$	$\cos \alpha / \cos \beta$	$\cos \alpha / \cos \beta$			
A	$\cot \beta$	$-\cot \beta$	$-\cot \beta$	$\cot \beta$	$\tan \beta$	$\tan \beta$

Strategy: scanning and experimental constraints

The input parameters:

- the physical Higgs boson masses (m_H, m_h, m_A, m_{H^\pm}),
- the vacuum expectation value ratio ($\tan \beta$),
- the CP-even Higgs mixing angle (α),
- m_{12}^2 .

With the above inputs, $\lambda_{1,2,3,4,5}$ as well as m_{11}^2 and m_{22}^2 are determined (the latter two via the minimization conditions).

We adopted (and modified) the 2HDMC code for branching ratio calculations (D. Eriksson, J. Rathsman and O. Stal, Comput. Phys. Commun. **181**, 189 (2010) [arXiv:0902.0851]).

Scanning scenarios

I. $m_h = 125 \text{ GeV}$

II. $m_H = 125 \text{ GeV}$

III. $m_h = m_H = 125 \text{ GeV}$

IV. $m_h = m_A = 125 \text{ GeV}$

V. $m_H = m_A = 125 \text{ GeV}$

	scenario I	scenario II	scenario III	scenario IV	scenario V
$m_h \text{ [GeV]}$	125	$\{10, \dots, 124.9\}$	125	125	$\{10, \dots, 124.9\}$
$m_H \text{ [GeV]}$	$125 + \{0.1, \dots, 1000\}$	125	125.1	$125 + \{0.1, \dots, 1000\}$	125
$m_A \text{ [GeV]}$	$\{10, \dots, 1000\}$	$\{10, \dots, 1000\}$	$\{10, \dots, 1000\}$	125.1	125.1
$m_{H^\pm} \text{ [GeV]}$	1500 ($\tan \beta = 0.5$); 800 ($\tan \beta = 1$); 350 ($\tan \beta = 2$); 90, 150, 250, 350 for Type I 600 ($\tan \beta = 0.5$); 500 ($\tan \beta = 1$); 340 ($\tan \beta = 2$); 320 for Type II				
$\tan \beta$	$\{0.5, \dots, 20\}$				
$\sin \alpha$	$\{-1, \dots, 1\}$				
$m_{12}^2 \text{ [GeV}^2]$	$\{-1000^2, \dots, 1000^2\}$				

Experimental constraints

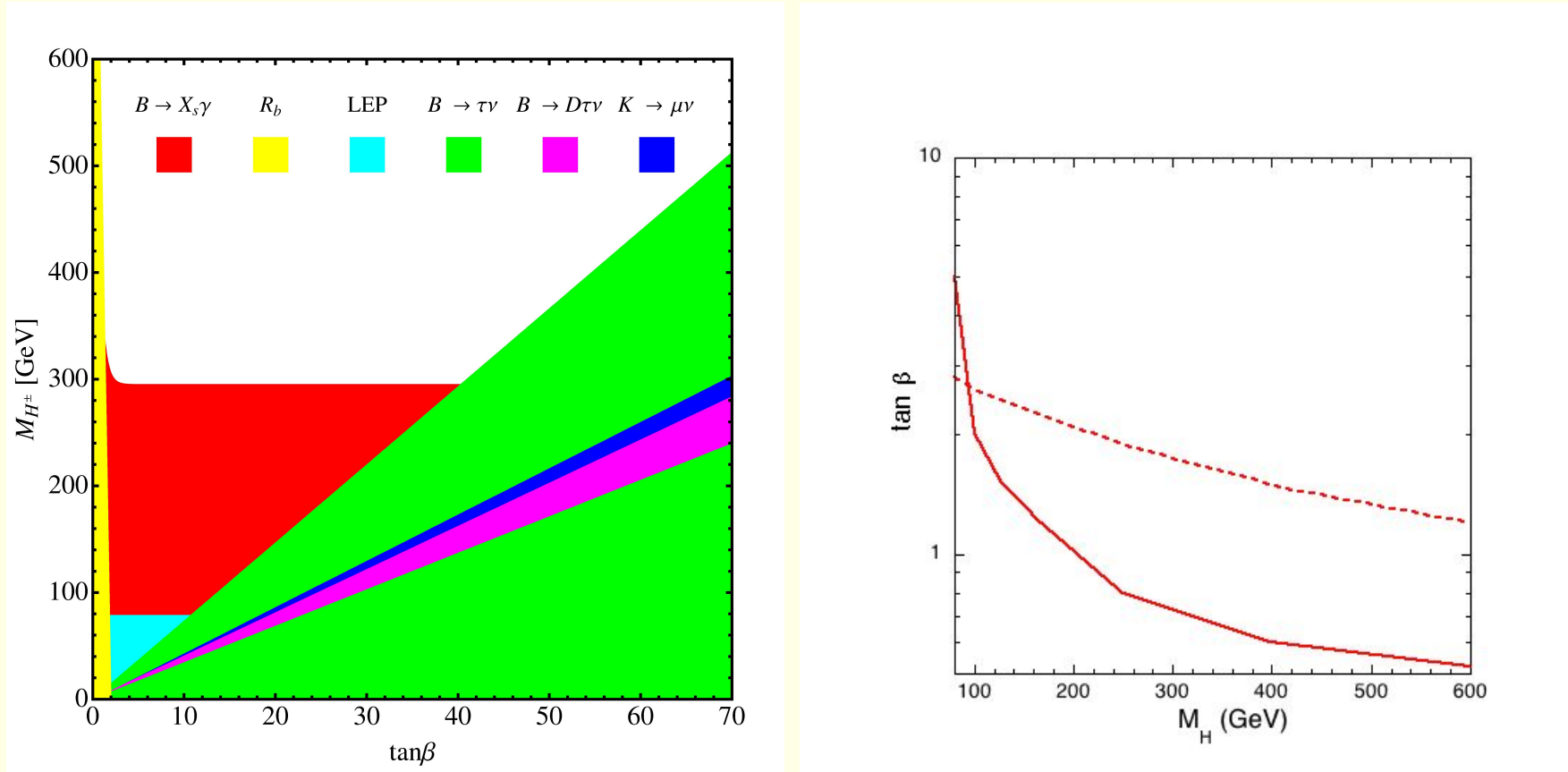


Figure 7: 1) Bounds in the m_{H^\pm} – $\tan\beta$ plane from various B-physics constraints for the type II model (U. Haisch, arXiv:0805.2141). 2) Lower bounds on $\tan\beta$ in the type I model as a function of the charged-Higgs mass m_{H^\pm} . The solid line is the bound is from $Z \rightarrow b\bar{b}, \epsilon_K$ and Δm_{B_s} (M. Jung, A. Pich and P. Tuzon, JHEP **1011**, 003 (2010), [arXiv:1006.0470]). The dashed line comes from $B \rightarrow \gamma X_s$ (F. Mahmoudi and O. Stal, Phys. Rev. D **81**, 035016 (2010) [arXiv:0907.1791]; R. S. Gupta and J. D. Wells, Phys. Rev. D **81**, 055012 (2010) [arXiv:0912.0267]).

Theoretical constraints:

- Perturbative unitarity: $|L_i| \leq 8\pi$
- Perturbativity: $|C_{H_i H_j H_k H_l}| \leq 4\pi$
- Vacuum stability: $\lambda_{1,2} > 0, \lambda_3 > -\sqrt{\lambda_1 \lambda_2}, \lambda_3 + \lambda_4 - |\lambda_5| > -\sqrt{\lambda_1 \lambda_2}$

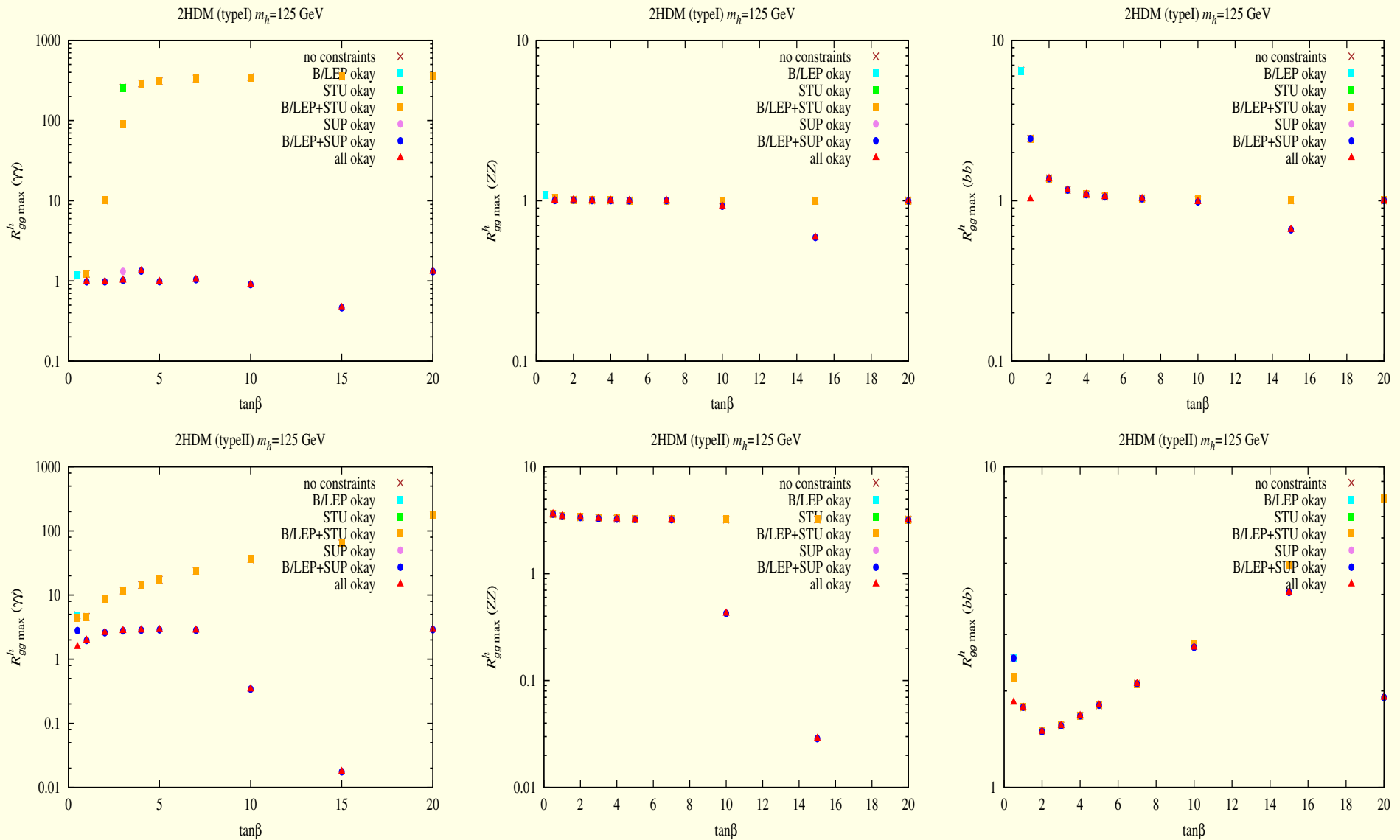


Figure 8: $R_{gg}^h(\gamma\gamma)$ maximum values and corresponding $R_{gg}^h(ZZ)$ and $R_{gg}^h(b\bar{b})$ as functions of $\tan\beta$ after imposing various constraints — see figure legend. Disappearance of a point after imposing a given constraint set means that the point did not satisfy that set of constraints. In a case of boxes and circles, if a given point satisfies subsequent constraints then the resulting color is chosen according to the color ordering shown in the legend.

$\tan \beta$	$R_{gg\max}^h(\gamma\gamma)$	$R_{gg}^h(ZZ)$	$R_{gg}^h(b\bar{b})$	$R_{VBF}^h(\gamma\gamma)$	$R_{VBF}^h(ZZ)$	$R_{VBF}^h(b\bar{b})$	m_H	m_A	m_{H^\pm}	m_{12}	$\sin \alpha$	$\mathcal{A}_{H^\pm}^h / \mathcal{A}$	δa_μ
1.0	0.98	1.00	1.02	0.96	0.98	1.00	875	750	800	500	-0.7	-0.01	-2.3
2.0	0.98	0.98	0.92	1.04	1.04	0.98	425	500	350	200	-0.5	-0.01	-1.8
3.0	1.02	0.98	0.92	1.08	1.04	0.98	225	400	150	100	-0.4	0.01	-1.7
4.0	1.33	0.99	1.07	1.24	0.93	0.99	225	200	90	100	-0.1	0.14	-1.7
5.0	0.98	0.98	1.06	0.90	0.91	0.98	225	400	150	100	-0.0	0.01	-1.6
7.0	1.04	0.99	0.98	1.06	1.01	0.99	135	500	90	50	-0.2	0.02	-1.6
10.0	0.90	0.81	0.74	0.99	0.89	0.81	175	500	150	50	-0.5	0.04	-1.5
15.0	0.46	0.59	0.66	0.41	0.53	0.59	225	400	350	50	0.6	-0.11	-1.4
20.0	1.31	1.00	1.00	1.30	0.99	1.00	225	200	90	50	-0.0	0.13	-1.5

Table 1: Table of maximum $R_{gg}^h(\gamma\gamma)$ values for Type I 2HDM with $m_h = 125$ GeV and associated input parameters.

$\tan \beta$	$R_{gg\max}^h(\gamma\gamma)$	$R_{gg}^h(ZZ)$	$R_{gg}^h(b\bar{b})$	$R_{VBF}^h(\gamma\gamma)$	$R_{VBF}^h(ZZ)$	$R_{VBF}^h(b\bar{b})$	m_H	m_A	m_{H^\pm}	m_{12}	$\sin \alpha$	$\mathcal{A}_{H^\pm}^h / \mathcal{A}$	δa_μ
0.5	1.56	2.69	1.84	0.52	0.89	0.61	425	500	600	100	-0.7	-0.06	-0.5
1.0	1.97	3.36	0.39	0.65	1.11	0.13	125	500	500	100	-0.2	-0.06	0.7
2.0	2.59	3.36	0.00	1.48	1.92	0.00	225	200	340	100	-0.0	-0.05	1.6
3.0	2.78	3.29	0.00	2.01	2.37	0.00	225	200	320	100	-0.0	-0.05	1.6
4.0	2.84	3.25	0.00	2.24	2.57	0.00	225	200	320	100	-0.0	-0.04	1.6
5.0	2.87	3.23	0.00	2.37	2.66	0.00	225	200	320	100	-0.0	-0.04	1.6
7.0	2.83	3.21	0.00	2.42	2.75	0.00	135	300	320	50	-0.0	-0.05	0.8
10.0	0.34	0.43	1.89	0.22	0.28	1.23	325	200	320	100	0.2	-0.08	3.5
15.0	0.02	0.03	4.06	0.00	0.01	0.87	225	200	320	50	0.6	-0.14	5.3
20.0	2.89	3.19	0.00	2.57	2.83	0.00	225	200	320	50	-0.0	-0.04	2.4

Table 2: Table of maximum $R_{gg}^h(\gamma\gamma)$ values for Type II 2HDM with $m_h = 125$ GeV and associated input parameters.

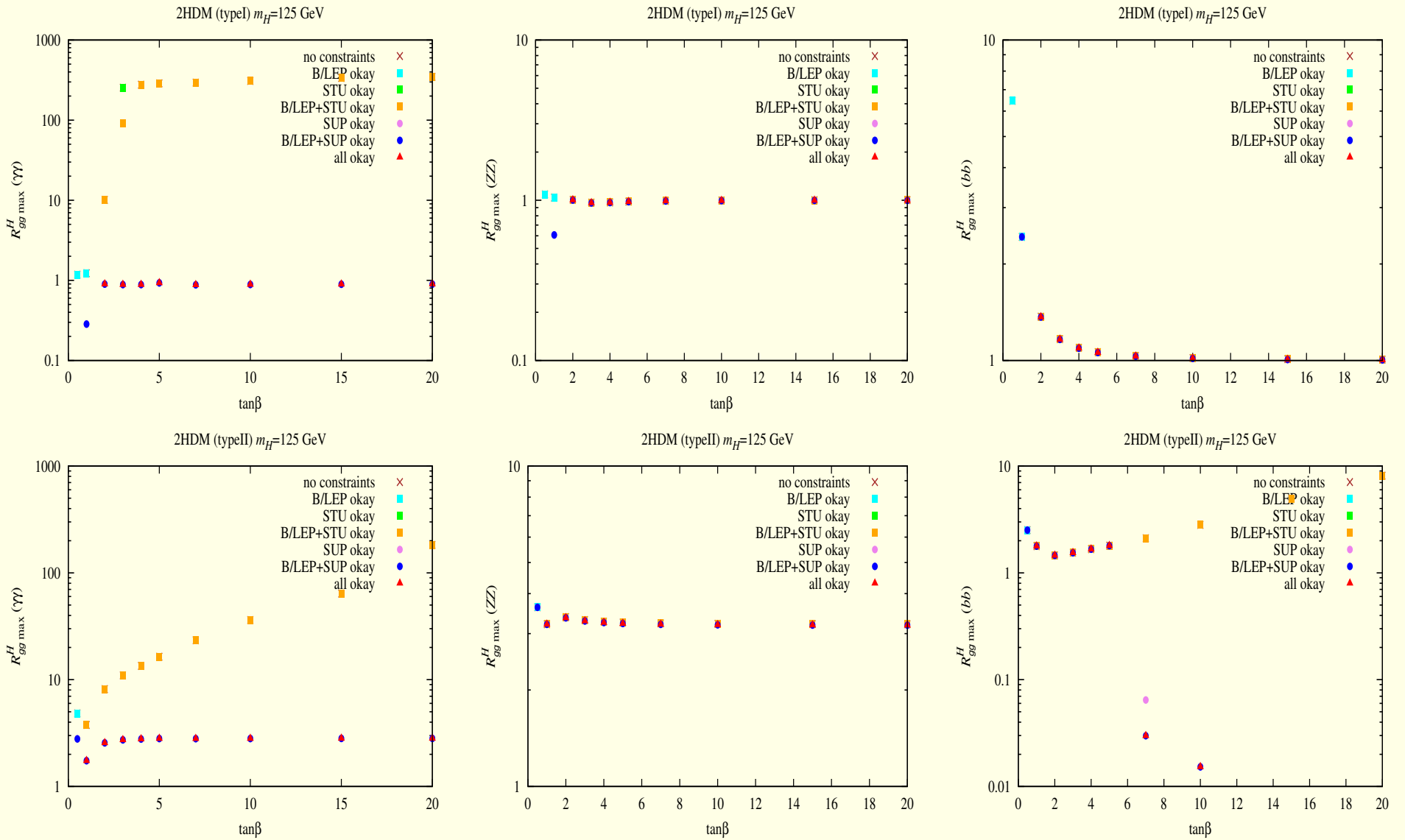


Figure 9: $R_{gg}^H(\gamma\gamma)$ maximum values and corresponding $R_{gg}^H(ZZ)$ and $R_{gg}^H(b\bar{b})$ as functions of $\tan\beta$ after imposing various constraints

— see figure legend. Disappearance of a point after imposing a given constraint set means that the point did not satisfy that set of constraints.

$\tan \beta$	$R_{gg\max}^H(\gamma\gamma)$	$R_{gg}^H(ZZ)$	$R_{gg}^H(b\bar{b})$	$R_{VBF}^H(\gamma\gamma)$	$R_{VBF}^H(ZZ)$	$R_{VBF}^H(b\bar{b})$	m_h	m_A	m_{H^\pm}	m_{12}	$\sin \alpha$	$\mathcal{A}_{H^\pm}/\mathcal{A}$	δa_μ
2.0	0.90	1.00	1.02	0.89	0.99	1.00	125	400	350	50	0.9	-0.05	-2.1
3.0	0.89	0.96	0.88	0.97	1.05	0.96	125	400	350	50	0.9	-0.05	-1.8
4.0	0.89	0.97	1.09	0.79	0.86	0.97	105	500	90	50	1.0	-0.03	-1.7
5.0	0.93	0.98	1.06	0.86	0.90	0.98	125	500	90	50	1.0	-0.01	-1.6
7.0	0.88	0.99	1.03	0.85	0.95	0.99	65	400	350	10	1.0	-0.05	-1.6
10.0	0.89	1.00	1.02	0.87	0.98	1.00	45	400	350	0	1.0	-0.05	-1.6
15.0	0.90	1.00	1.01	0.89	0.99	1.00	5	400	350	0	-1.0	-0.05	-1.6
20.0	0.90	1.00	1.00	0.89	0.99	1.00	25	400	350	0	-1.0	-0.05	-1.5

Table 3: Table of maximum $R_{gg}^H(\gamma\gamma)$ values for Type I 2HDM with $m_H = 125$ GeV and associated input parameters.

$\tan \beta$	$R_{gg\max}^H(\gamma\gamma)$	$R_{gg}^H(ZZ)$	$R_{gg}^H(b\bar{b})$	$R_{VBF}^H(\gamma\gamma)$	$R_{VBF}^H(ZZ)$	$R_{VBF}^H(b\bar{b})$	m_h	m_A	m_{H^\pm}	m_{12}	$\sin \alpha$	$\mathcal{A}_{H^\pm}/\mathcal{A}$	δa_μ
1.0	1.74	2.39	1.02	0.91	1.24	0.53	105	500	500	100	0.9	-0.06	0.8
2.0	2.56	3.36	0.00	1.46	1.92	0.00	125	300	340	50	1.0	-0.06	1.1
3.0	2.73	3.29	0.00	1.97	2.37	0.00	125	300	320	50	1.0	-0.05	1.0
4.0	2.78	3.25	0.00	2.20	2.57	0.00	125	300	320	50	-1.0	-0.05	1.0
5.0	2.81	3.23	0.00	2.32	2.66	0.00	125	300	320	50	-1.0	-0.05	0.9
7.0	2.80	3.21	0.00	2.40	2.75	0.00	65	300	320	10	-1.0	-0.06	-0.0
10.0	2.81	3.20	0.00	2.46	2.79	0.00	45	300	320	0	-1.0	-0.06	-2.8
15.0	2.82	3.19	0.00	2.49	2.82	0.00	25	300	320	0	-1.0	-0.05	-16.9
20.0	2.82	3.19	0.00	2.50	2.83	0.00	25	300	320	0	-1.0	-0.05	-30.8

Table 4: Table of maximum $R_{gg}^H(\gamma\gamma)$ values for Type II 2HDM with $m_H = 125$ GeV and associated input parameters.

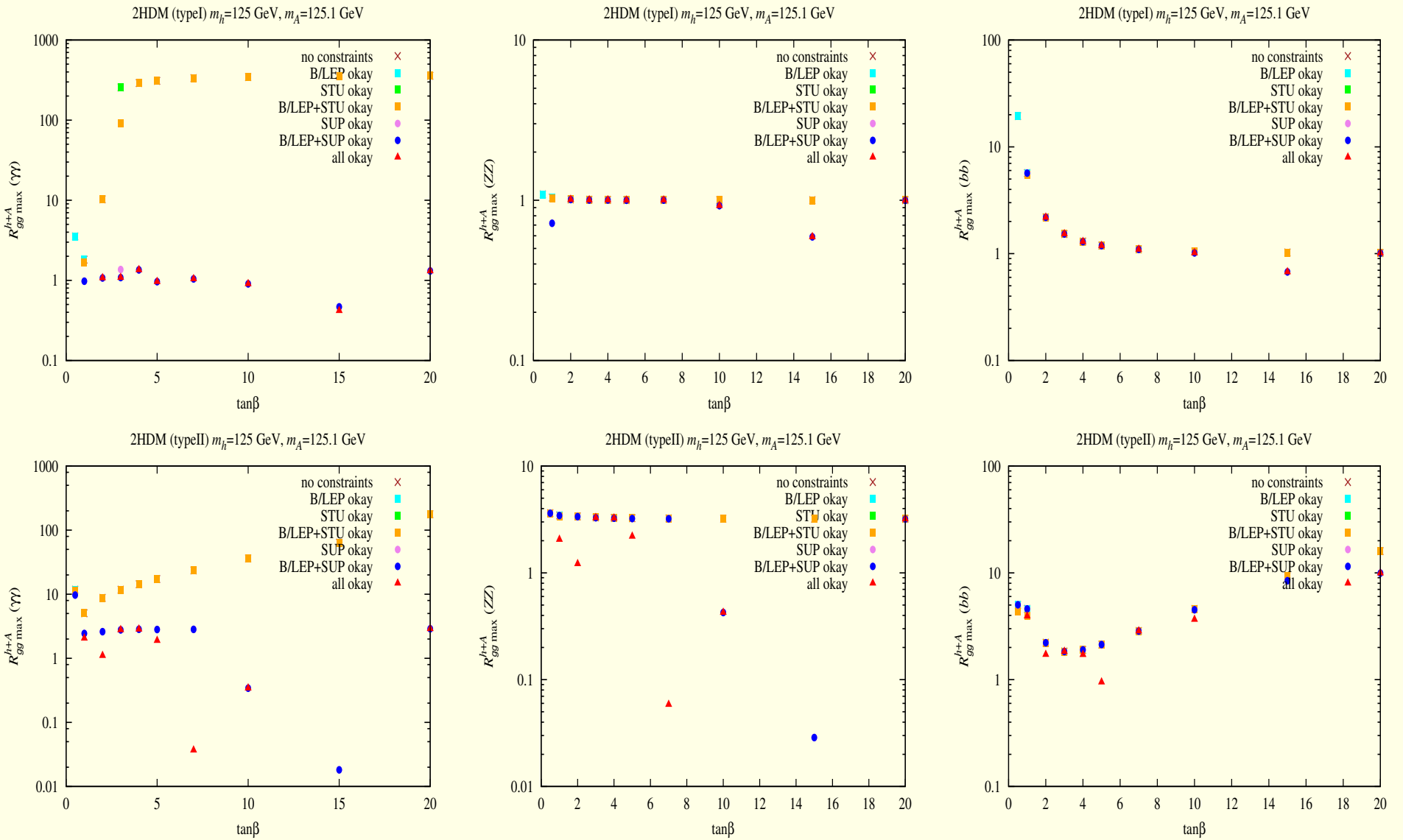


Figure 10: $R_{gg}^{h+A}(\gamma\gamma)$ maximum values when $m_h \simeq m_A = 125$ GeV and corresponding $R_{gg}^{h+A}(ZZ)$ and $R_{gg}^{h+A}(b\bar{b})$ as functions of $\tan\beta$ after imposing various constraints — see figure legend. Disappearance of a point after imposing a given constraint set means that the point did not satisfy that set of constraints.

$\tan \beta$	$R_{gg\max}^{h+A}(\gamma\gamma)$	$R_{gg}^h(\gamma\gamma)$	$R_{gg}^A(\gamma\gamma)$	$R_{gg}^{h+A}(ZZ)$	$R_{gg}^{h+A}(b\bar{b})$	$R_{VBF}^h(\gamma\gamma)$	$R_{VBF}^h(ZZ)$	$R_{VBF}^h(b\bar{b})$	m_H	m_{H^\pm}	m_{12}	$\sin \alpha$	$\mathcal{A}_{H^\pm}^h/\mathcal{A}$	δa_μ
2.0	1.07	0.92	0.15	0.98	1.73	0.98	1.04	0.98	325	250	100	-0.5	-0.04	-2.2
3.0	1.08	1.02	0.07	0.98	1.28	1.08	1.04	0.98	225	150	100	-0.4	0.01	-1.9
4.0	1.35	1.33	0.03	0.99	1.21	1.24	0.93	0.99	225	90	100	-0.1	0.14	-1.8
5.0	0.96	0.95	0.01	1.00	1.07	0.95	1.00	1.00	135	90	50	-0.2	-0.03	-1.7
7.0	1.04	1.04	0.01	0.99	1.00	1.06	1.01	0.99	135	90	50	-0.2	0.02	-1.6
10.0	0.91	0.90	0.01	0.81	0.77	0.99	0.89	0.81	175	150	50	-0.5	0.04	-1.5
15.0	0.42	0.42	0.00	0.59	0.67	0.37	0.53	0.59	225	250	50	0.6	-0.17	-1.4
20.0	1.31	1.31	0.00	1.00	1.00	1.30	0.99	1.00	225	90	50	-0.0	0.13	-1.6

Table 5: Table of maximum $R_{gg}^{h+A}(\gamma\gamma)$ values for Type I 2HDM with $m_h = m_A = 125$ GeV and associated input parameters.

$\tan \beta$	$R_{gg\max}^{h+A}(\gamma\gamma)$	$R_{gg}^h(\gamma\gamma)$	$R_{gg}^A(\gamma\gamma)$	$R_{gg}^{h+A}(ZZ)$	$R_{gg}^{h+A}(b\bar{b})$	$R_{VBF}^h(\gamma\gamma)$	$R_{VBF}^h(ZZ)$	$R_{VBF}^h(b\bar{b})$	m_H	m_{H^\pm}	m_{12}	$\sin \alpha$	$\mathcal{A}_{H^\pm}^h/\mathcal{A}$	δa_μ
1.0	2.05	1.58	0.47	2.05	3.91	0.93	1.22	0.65	525	500	100	-0.5	-0.06	1.3
2.0	1.10	1.09	0.01	1.21	1.69	1.02	1.14	0.91	325	340	100	-0.4	-0.05	1.5
3.0	2.78	2.78	0.00	3.29	0.27	2.01	2.37	0.00	225	320	100	-0.0	-0.05	2.3
4.0	2.84	2.84	0.00	3.25	0.23	2.24	2.57	0.00	225	320	100	-0.0	-0.04	2.3
5.0	1.89	1.89	0.00	2.19	0.95	1.41	1.64	0.47	225	320	100	0.1	-0.05	2.7
7.0	0.04	0.04	0.00	0.06	2.85	0.01	0.02	0.75	325	320	100	0.6	-0.15	5.2
10.0	0.34	0.34	0.00	0.43	3.66	0.22	0.28	1.23	325	320	100	0.2	-0.08	4.7
20.0	2.89	2.89	0.00	3.19	8.03	2.57	2.83	0.00	225	320	50	-0.0	-0.04	5.6

Table 6: Table of maximum $R_{gg}^{h+A}(\gamma\gamma)$ values for Type II 2HDM with $m_h = m_A = 125$ GeV and associated input parameters.

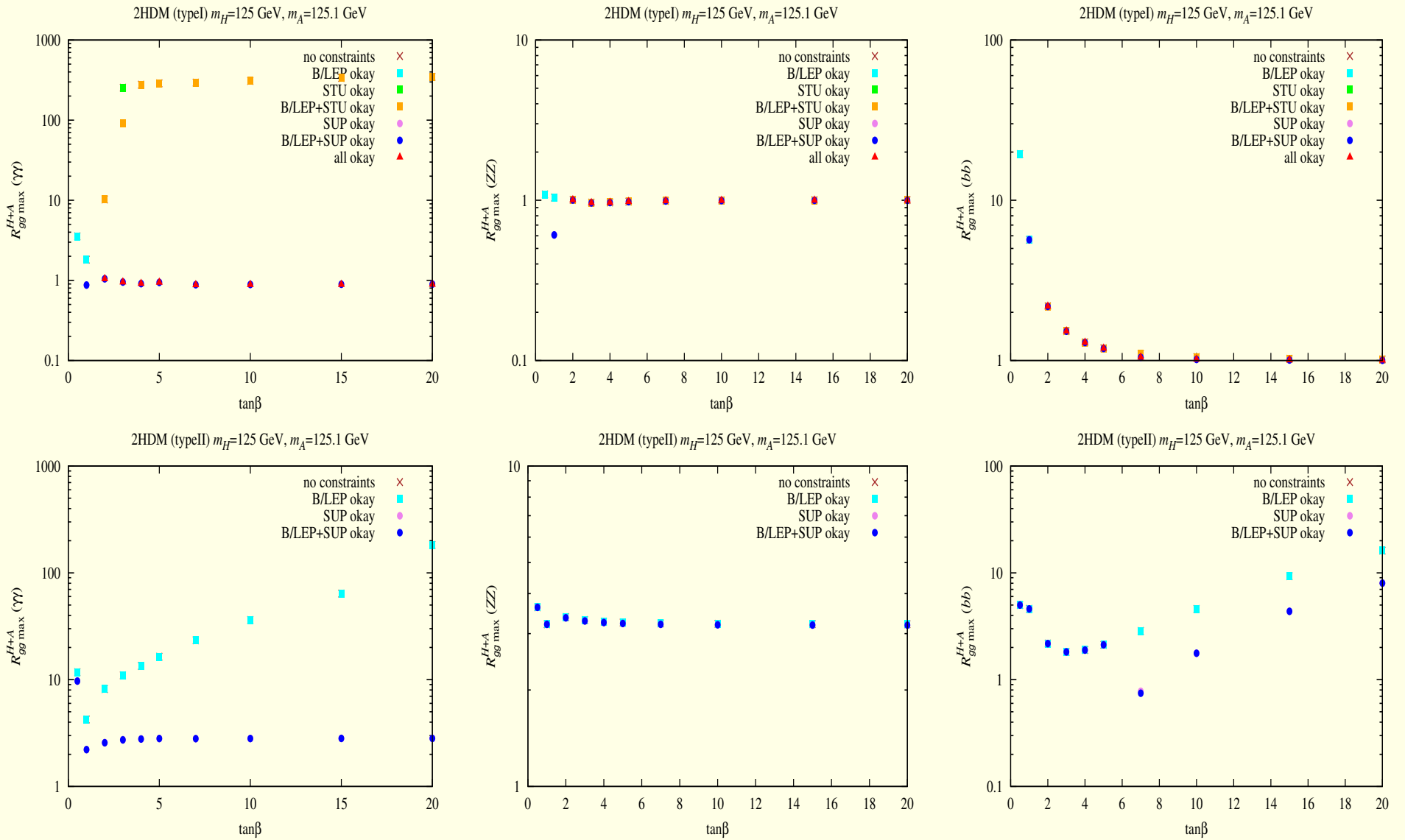


Figure 11: $R_{gg}^{H+A}(\gamma\gamma)$ maximum values when $m_H \simeq m_A = 125$ GeV and corresponding $R_{gg}^{H+A}(ZZ)$ and $R_{gg}^{H+A}(bb)$ as functions of $\tan\beta$ after imposing various constraints — see figure legend. Disappearance of a point after imposing a given constraint set means that the point did not satisfy that set of constraints.

$\tan \beta$	$R_{gg\max}^{H+A}(\gamma\gamma)$	$R_{gg}^H(\gamma\gamma)$	$R_{gg}^A(\gamma\gamma)$	$R_{gg}^{H+A}(ZZ)$	$R_{gg}^{H+A}(b\bar{b})$	$R_{\text{VBF}}^H(\gamma\gamma)$	$R_{\text{VBF}}^H(ZZ)$	$R_{\text{VBF}}^H(b\bar{b})$	m_h	m_{H^\pm}	m_{12}	$\sin \alpha$	$\mathcal{A}_{H^\pm}^H/\mathcal{A}$	δa_μ
2.0	1.04	0.90	0.15	1.00	1.83	0.88	0.99	1.00	125	250	50	0.9	-0.06	-2.5
3.0	0.95	0.88	0.07	0.96	1.24	0.97	1.05	0.96	125	250	50	0.9	-0.06	-2.0
4.0	0.91	0.89	0.03	0.97	1.23	0.79	0.86	0.97	125	90	50	1.0	-0.03	-1.8
5.0	0.94	0.93	0.01	0.98	1.13	0.86	0.90	0.98	125	90	50	1.0	-0.01	-1.7
7.0	0.88	0.87	0.00	0.99	1.05	0.84	0.95	0.99	65	150	10	1.0	-0.06	-1.6
10.0	0.88	0.88	0.00	1.00	1.02	0.86	0.98	1.00	45	150	0	-1.0	-0.06	-1.6
15.0	0.89	0.89	0.00	1.00	1.01	0.88	0.99	1.00	25	150	0	-1.0	-0.06	-1.6
20.0	0.89	0.89	0.00	1.00	1.00	0.88	0.99	1.00	25	150	0	-1.0	-0.06	-1.6

Table 7: Table of maximum $R_{gg}^{H+A}(\gamma\gamma)$ values for Type I 2HDM with $m_H = m_A = 125$ GeV and associated input parameters.

$\tan \beta$	$R_{gg\max}^{h+H}(\gamma\gamma)$	$R_{gg}^h(\gamma\gamma)$	$R_{gg}^H(\gamma\gamma)$	$R_{gg}^{h+H}(ZZ)$	$R_{gg}^{h+H}(b\bar{b})$	$R_{\text{VBF}}^{h+H}(\gamma\gamma)$	$R_{\text{VBF}}^{h+H}(ZZ)$	$R_{\text{VBF}}^{h+H}(b\bar{b})$	m_A	m_{H^\pm}	m_{12}	$\sin \alpha$	$\mathcal{A}_{H^\pm}^h/\mathcal{A}$	δa_μ
2.0	0.96	0.87	0.10	1.04	1.32	0.76	0.87	1.04	400	350	50	-0.3	-0.06	-2.1
3.0	0.93	0.88	0.05	1.02	1.14	0.83	0.93	1.02	400	350	50	-0.2	-0.05	-1.8
4.0	0.92	0.92	0.00	1.00	1.06	0.90	0.98	1.00	500	90	50	-0.2	-0.04	-1.7
5.0	0.95	0.95	0.00	1.00	1.04	0.92	0.96	1.00	500	90	50	-0.1	-0.02	-1.6

Table 8: Table of maximum $R_{gg}^{h+H}(\gamma\gamma)$ values for Type I 2HDM with $m_h = m_H = 125$ GeV and associated input parameters.

$\tan \beta$	$R_{gg\max}^{h+H}(\gamma\gamma)$	$R_{gg}^h(\gamma\gamma)$	$R_{gg}^H(\gamma\gamma)$	$R_{gg}^{h+H}(ZZ)$	$R_{gg}^{h+H}(b\bar{b})$	$R_{\text{VBF}}^{h+H}(\gamma\gamma)$	$R_{\text{VBF}}^{h+H}(ZZ)$	$R_{\text{VBF}}^{h+H}(b\bar{b})$	m_A	m_{H^\pm}	m_{12}	$\sin \alpha$	$\mathcal{A}_{H^\pm}^h/\mathcal{A}$	δa_μ
1.0	2.08	1.96	0.11	3.09	1.12	0.87	1.25	0.59	500	500	100	-0.3	-0.06	0.7
2.0	2.57	2.56	0.01	3.36	0.09	1.48	1.93	0.30	300	340	50	-0.0	-0.06	1.1
3.0	2.74	2.73	0.00	3.29	0.19	1.98	2.38	0.15	300	320	50	-0.0	-0.05	1.0
4.0	2.79	2.78	0.00	3.25	0.32	2.20	2.57	0.09	300	320	50	-0.0	-0.05	1.0
5.0	2.81	2.81	0.00	3.23	0.48	2.32	2.66	0.06	300	320	50	-0.0	-0.05	0.9

Table 9: Table of maximum $R_{gg}^{h+H}(\gamma\gamma)$ values for Type II 2HDM with $m_h = m_H = 125$ GeV and associated input parameters.

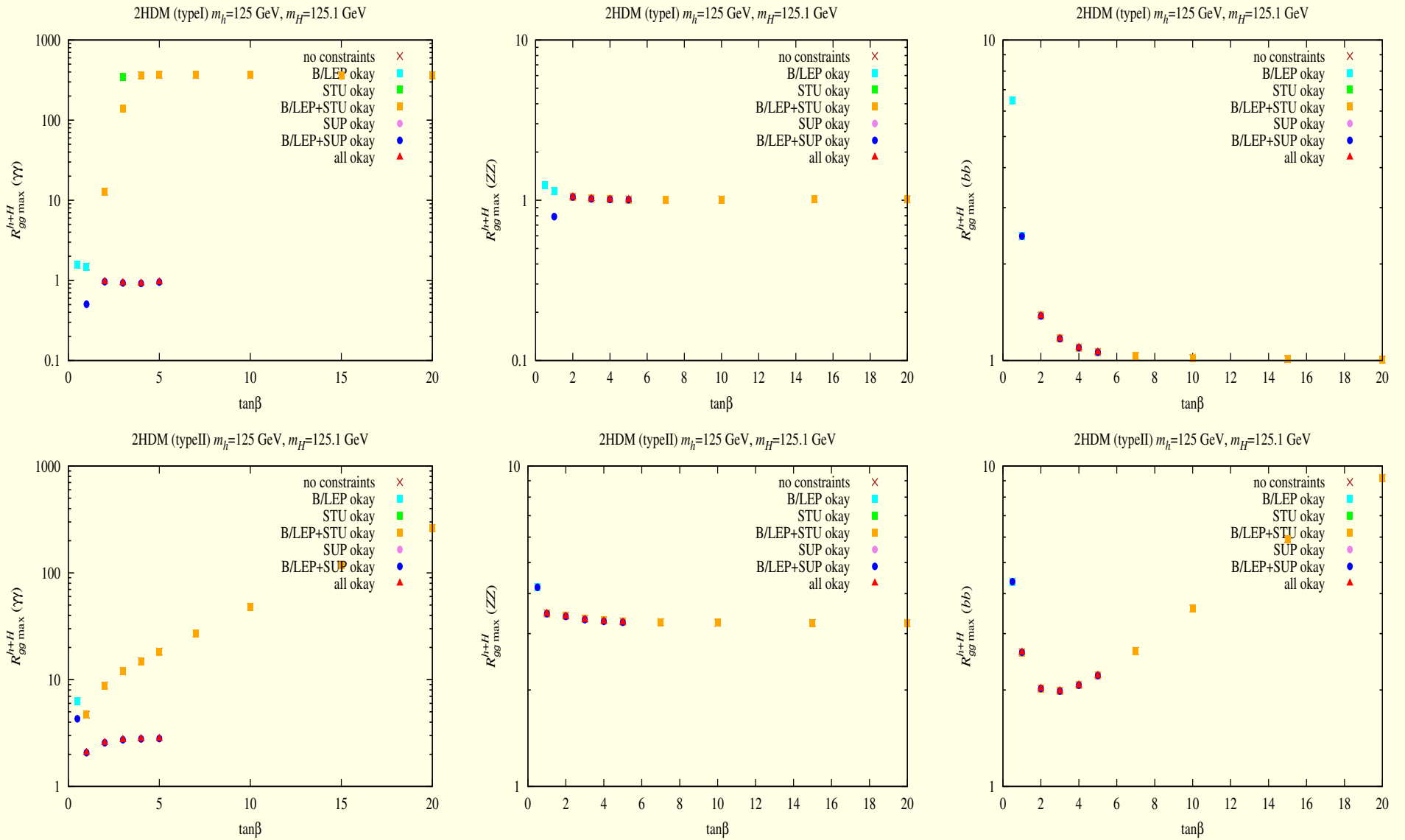


Figure 12: $R_{gg}^{h+H}(\gamma\gamma)$ maximum values when $m_h \simeq m_H = 125$ GeV and corresponding $R_{gg}^{h+H}(ZZ)$ and $R_{gg}^{h+H}(b\bar{b})$ functions of $\tan\beta$ after imposing various constraints — see figure legend. Disappearance of a point after imposing a given constraint set means that the point did not satisfy that set of constraints.

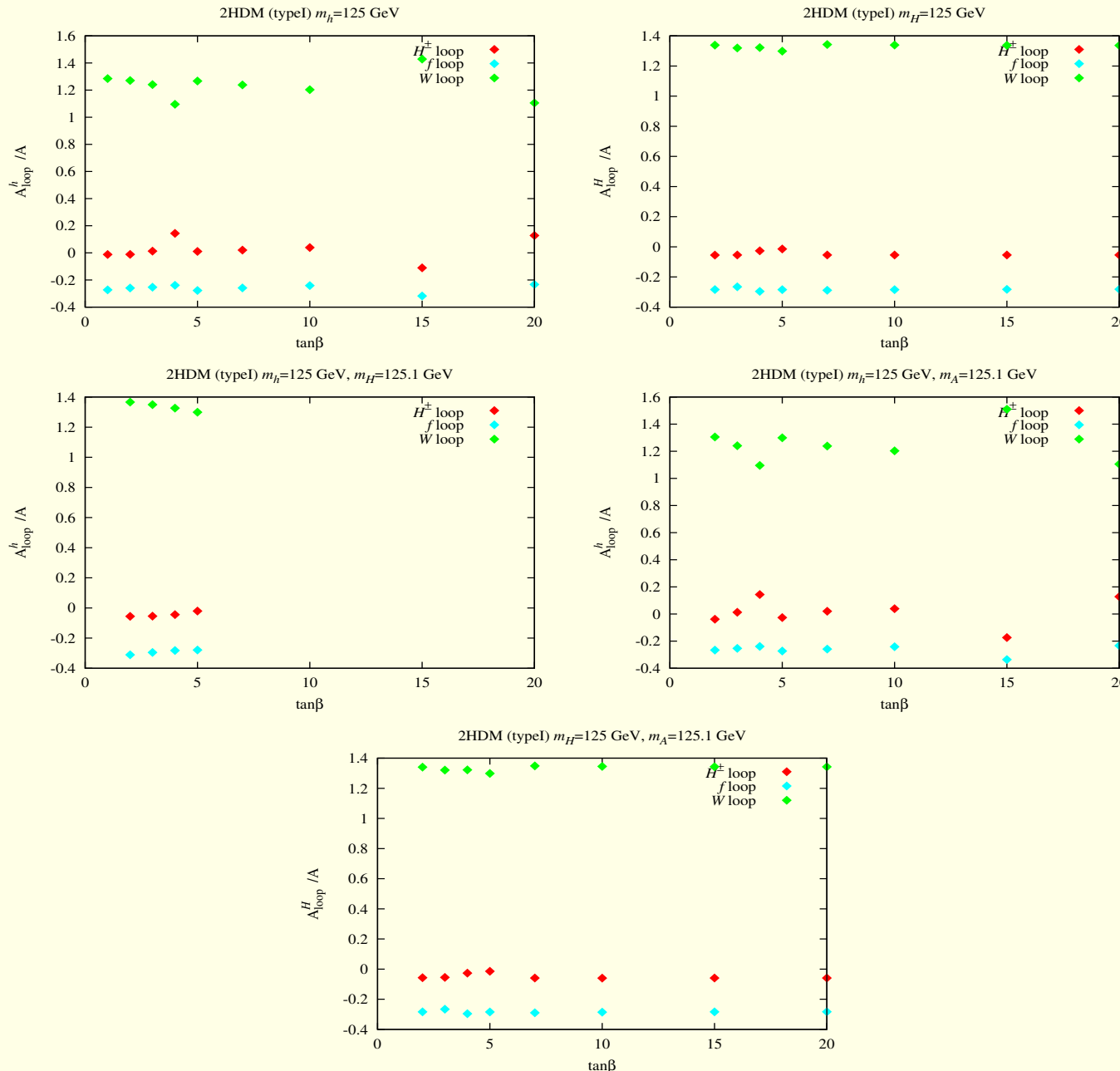


Figure 13: Imaginary part of charged Higgs, fermionic and W contributions to the $\gamma\gamma$ amplitude for the type I model normalized to the imaginary part of the sum of all (fermions, W^+W^- , H^+H^-) contributions as a function of $\tan \beta$ after imposing all constraints. The parameters adopted correspond to maximal $R_{gg}^{hi}(\gamma\gamma)$ (or an appropriate sum for degenerate cases).

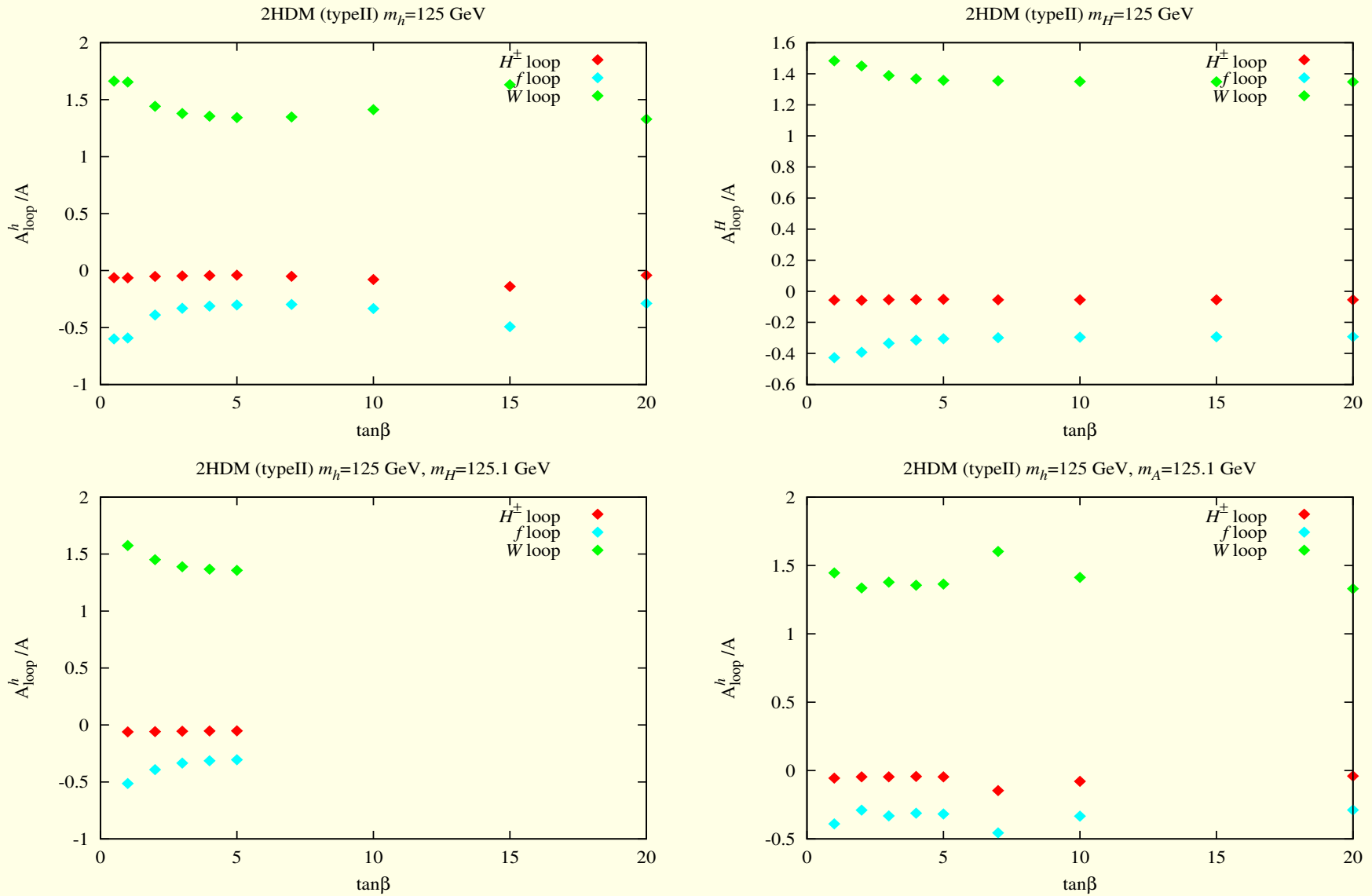


Figure 14: Imaginary part of charged Higgs, fermionic and W contributions to the $\gamma\gamma$ amplitude for the type II model normalized to the imaginary part of the sum of all (fermions, W^+W^- , H^+H^-) contributions as a function of $\tan\beta$ after imposing all constraints. The parameters adopted correspond to maximal $R_{gg}^{h_i}(\gamma\gamma)$ (or an appropriate sum for degenerate cases).

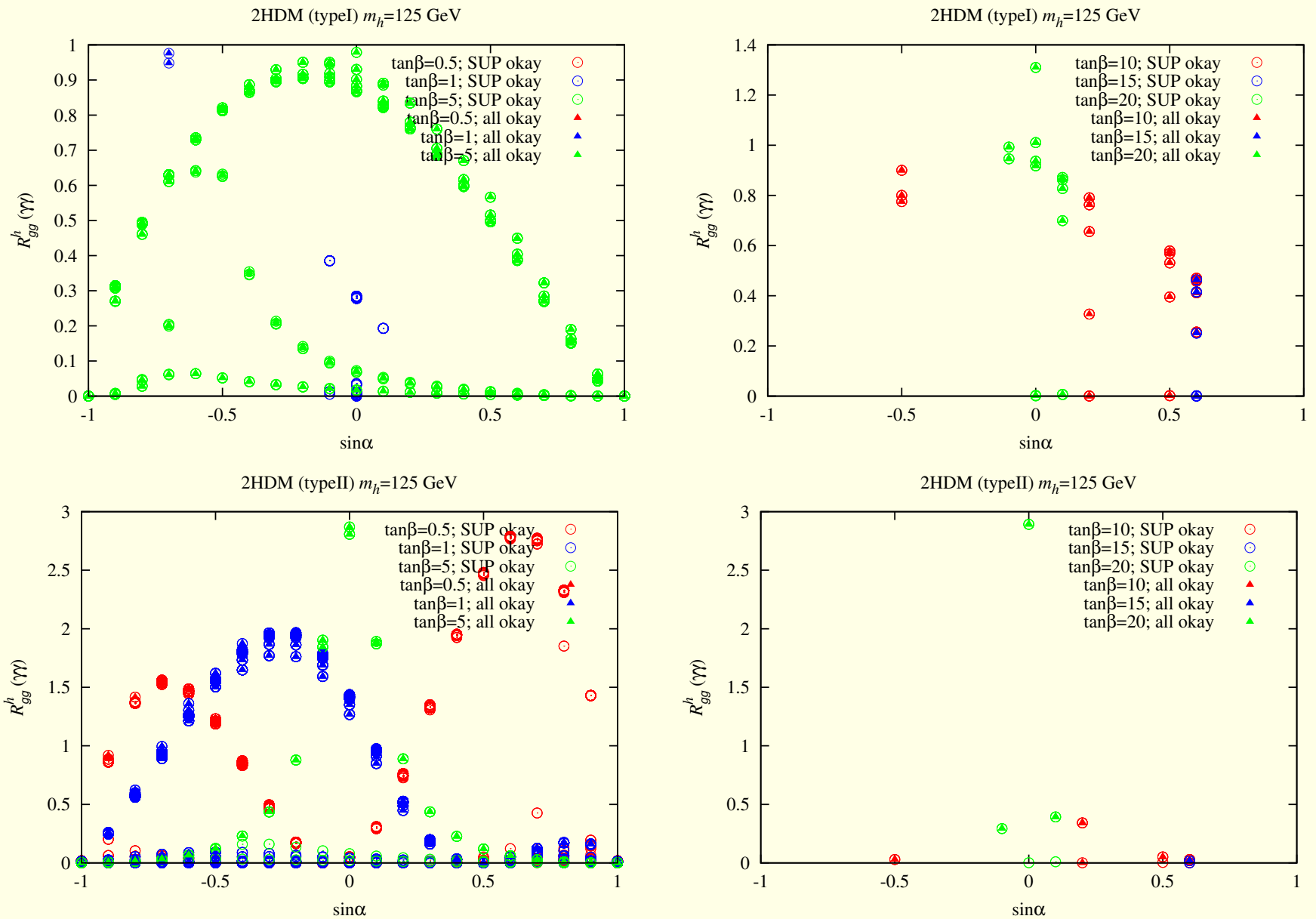


Figure 15: $R_{gg}^h(\gamma\gamma)$ is plotted as a function of $\sin \alpha$ for a sequence of $\tan \beta$ values. Different constraint combinations are considered and the different curves of given type correspond to a variety of other input parameters. The upper plots are for the Type I model and the lower plots are for the Type II model. Different colors indicate different $\tan \beta$ values.

Conclusions on the 2HDM, type I and II setup:

- Easier to enhance $R_{gg}^{h_i}$ for the type II model:

- $R_{gg \max}^{h_i \text{ type II}}(\gamma\gamma) \lesssim 3$,
- $R_{gg \max}^{h_i \text{ type I}}(\gamma\gamma) \lesssim 1.5$.

- Type II model implies too strong ZZ signal:

$$1 < R_{gg \max}^{h_i \text{ type II}}(\gamma\gamma) \lesssim R_{gg \max}^{h_i \text{ type II}}(ZZ) \sim 2 - 3.5$$

- Optimal signal for the type I model for $\tan\beta = 4, 20$ within the scenarios: I ($m_h = 125$ GeV) and IV ($m_h = m_A = 125$ GeV).
- H^\pm effects up to $\sim 20\%$.

Summary

- The off-brane RS scenario with R -Higgs mixing offers a realistic explanation for the recent LHC data for:
 - Un-fixed Λ_ϕ scenario, signal at only 125 GeV ($m_h = 125$ GeV and $m_\phi = 120$ GeV) for $m_0/m_{Pl} = 0.4$ and $\xi \sim -0.09$.
 - Fixed $\Lambda_\phi = 1$ TeV scenario, signal at only 125 GeV ($m_h = 120$ GeV and $m_\phi = 125$ GeV) for $m_0/m_{Pl} = 1$ and $\xi \sim -0.016$.
 - Signal (h or ϕ) at 125 GeV and high mass: no consistent and interesting solution.
- 2HDM's type I and II:
 - Consistent fit to the signal seen at the LHC. Data seem to favour the type I model with $\tan\beta = 4, 20$, $m_H = 225$ GeV, $m_A = 200$ GeV, $m_{H^\pm} = 90$ GeV, $m_{12} = 100, 50$ GeV and $\sin\alpha = -0.1, 0.0$.